Soil Constitutive Model for Geotechnical Design against Geo-hazards

William Higgins and Dipanjan Basu
Department of Civil and Environmental Engineering, University of Connecticut, Storrs, CT, USA.
Tanusree Chakraborty
Department of Civil Engineering, Indian Institute of Technology Delhi, New Delhi, India.

ABSTRACT
Natural disasters like landslide, mudflow and debris flow often cause catastrophic failures in civil infrastructure and may give rise to high rates of strain (10^2-10^4/sec) in soil. The rate of induced strain (or stress) has a significant effect on the strength and stiffness of soil. In this paper, the high strain-rate behavior of sand is investigated by developing a rate-dependent, viscoplastic two-surface constitutive model. The model is based on the concepts of critical-state soil mechanics. It captures the behavior of sand under multi-axial loading conditions, predicts both the drained and undrained responses at small and large strains, and reproduces the critical state, peak strength and dilatancy behavior of sand. Perzyna's overstress theory is incorporated in this model to reproduce the viscoplastic sand behavior under high loading rate. Particle crushing is captured by incorporating a flat cap to the bounding surface. A nonassociated flow rule is assumed. The rate-dependent model parameters are determined from the experimental data of split Hopkinson pressure bar (SHPB) tests under high rate loading. The performance of the model in simulating the high strain-rate mechanical response of sand in SHPB tests is demonstrated for different initial states and loading conditions.

RÉSUMÉ
Les désastres naturels comme le glissement de terrain, mudflow et le débris coulent souvent les défaillances irrémédiables de cause dans l'infrastructure civile et peuvent engendrer d'hauts taux de tension (102-104/sec) dans le sol. Le taux de tension induite (ou la tension) a un effet significatif sur la force et la raideur de sol. Dans ce papier, l'haut comportement de tension-taux de sable est examiné en développant une dépendante du taux, la deux-surface de viscoplastic le modèle constituant. Le modèle est fondé sur les concepts de mécanique de sol de critique-état. Il capture le comportement de sable sous les conditions de chargement multi-axiaux, prédit les drainé et undrained réponses aux petites et grandes tensions, et reproduit l'état critique, la force maximum et le comportement de dilatancy de sable. Perzyna trop souligne la théorie est incorporée dans ce modèle pour reproduire le comportement de sable de viscoplastic sous chargeant haut le taux. Ecraser de particule est capturé en incorporant un bouchon plat à la surface limitée. Une règle de flux de nonassociated est supposée. Les paramètres modèles dépendants du taux sont déterminés des données expérimentales d'a fractionné la barre de pression de Hopkinson (SHPB) les tests sous l'haut chargement de taux. L'exécution du modèle dans simuler l'haut tension-taux la réponse mécanique de sable dans les tests de SHPB est démontrée pour les états et les conditions de chargement initiaux différents.
.

1 INTRODUCTION

Natural hazards like landslide, mudflow, debris flow, earthquake and tsunami and man-made hazards like bomb blast and collision cause catastrophic failures in civil infrastructure. Hazardous flows (e.g., landslide, mudflow and debris flow) can move rapidly with a speed as high as 0.03 km/sec. Earthquake induced P and S wave speed can be up to 6 km/sec (Kumar et al. 1987, Tseng and Chen 2004). A bomb blast can create strain rates in materials up to 10^4/sec (DeSilva 2005, Barsoum and Philip 2007, Ishihara 1996). Often, large geo-structures like earth embankments, slopes and tunnels involving large masses of soil are affected by these hazards that generate high rates of strain, of the order of 10^2-10^4/sec, in the soil. Soil is the weakest of all civil engineering materials and often collapse of a civil engineering structure is initiated from within the soil. In order to safeguard civil engineering facilities against different catastrophic hazards, it is essential that soils subjected to high strain rates are properly characterized and modeled. The rate of induced strain (or stress) plays a significant effect on the strength and stiffness of soil.

Casagrande and Shannon (1948) were the first to study the effect of strain rate on the strength of soil. They performed drained triaxial compression tests on dense Manchester sand with strain rates varying from 10^{-5}/sec to 1/sec and observed that the compressive strength of sand increased by about 10% from the corresponding rate-independent (static) value. Since then, many researchers have performed drained and undrained triaxial tests on sand under different loading rates (Whitman and Healy 1962, Yamamuro and Lade 1998, Yamamuro and Abrantes 2003). Jackson et al. (1980) conducted uniaxial strain tests on sand at 200/sec strain rate. It was observed from these triaxial and uniaxial tests that the shear strength of sand increases by about 10% with each log-cycle increase in the strain rate and that an increase in the

applied rate of strain results in increased dilatancy and earlier peak generation. It was further observed that the dynamic shear modulus of sand was 5-40% greater than the static shear modulus. The split Hopkinson pressure bar (SHPB) tests have been performed on sand by several researchers in order to investigate sand behavior at strain rates as high as 10^4/sec (Felice 1985, Veyera and Ross 1995, Semblat et al. 1999, Song et al. 2009). The results show that the compressive response of dry sand is dependent on the initial density, compaction and lateral confinement. The stress-strain response of highly saturated sand (with the degree of saturation > 80%) in SHPB tests exhibits an initial steep portion in the stress-strain plot.

Only a few researchers (Laine and Sandvik 2001, Wang et al. 2004, Grujicic et al. 2006, Tong and Tuan 2007, Deshpande et al. 2009) have attempted to develop soil constitutive models for high strain rates. Although some of the existing constitutive models can capture strain rates as high as 200/sec and have been applied to simulate blast loading in soil, they are mostly not capable of capturing the stress-path dependent, multi-axial soil behavior with all the important features like the peak and critical states and phase transformation under both rate-independent and rate-dependent loading.

In this paper, a rate-dependent, viscoplastic constitutive model for sand is developed that can simulate all the important features, e.g., dilatancy, critical state and phase transformation, of the multi-axial, stress-path dependent behavior of sand under both drained and undrained loading and can capture extremely high strain rates. The model is developed by extending the modified Manzari-Dafalias two-surface plasticity model for sands (Manzari and Dafalias 1997, Papadimitriou and Bouckovalas 2001, Dafalias and Manzari 2004, Loukidis and Salgado 2009). Viscoplasticity is incorporated in the model using Perzyna's overstress theory (Perzyna 1963 and 1966). Crushing of sand particles under high loading rate is captured through the incorporation of a flat cap to the bounding surface. The strain-rate dependence of the shear modulus is incorporated explicitly in the model. The model performance is demonstrated by comparing the test results obtained from high-speed SHPB tests for up to 2000/sec strain rate with the corresponding simulation results.

2 BASIC PLASTICITY MODEL

The rate-independent, two-surface sand plasticity model adopted in the study was proposed by Manzari and Dafalias (1997) and later modified by Loukidis and Salgado (2009). Figure 1 shows the model in the normalized deviatoric stress space. The model contains four conical shear surfaces, the yield, bounding, dilatancy and critical-state (CS) surfaces, with straight surface meridians and apex at the origin. The projection and interpolation rules are exclusively contained in the deviatoric plane. The yield surface of the model is given by

$$f = \sqrt{\rho_{ij}\rho_{ij}} - \sqrt{2/3}\,m = 0 \qquad (1)$$

where m is the radius of the yield surface and ρ_{ij} is the stress ratio given by

$$\rho_{ij} = r_{ij} - \alpha_{ij} \qquad (2)$$

in which r_{ij} is the normalized deviatoric stress tensor ($r_{ij} = s_{ij}/p'$; s_{ij} is the deviatoric stress tensor and p' is the effective mean stress) and α_{ij} is the kinematic hardening tensor.

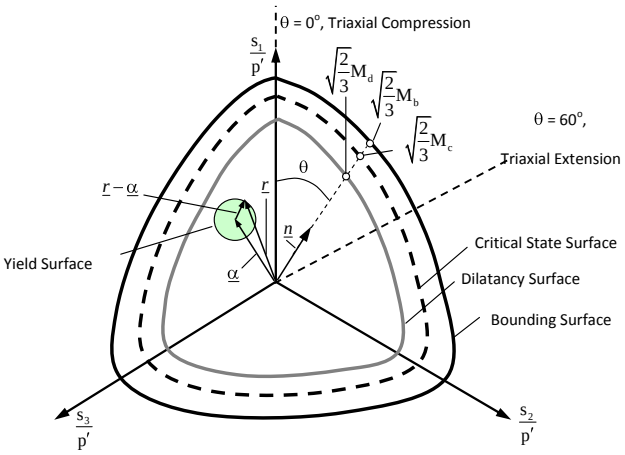

Figure 1. Modified Manzari-Dafalias two-surface plasticity model for sand (from Loukidis and Salgado 2009)

The yield surface can harden only kinematically through the use of the kinematic hardening tensor α_{ij}. The bounding and the dilatancy surfaces can harden or soften isotropically through the dependence of the corresponding stress ratios M_b and M_d on the state parameter ψ (ψ = e – e_c; where e and e_c are the current and critical-state void ratios at the same mean stress) (Been and Jefferies 1985) as

$$M_b = g(\theta)M_{cc}e^{-k_b\psi} \qquad (3)$$

$$M_d = g(\theta)M_{cc}e^{k_d\psi} \qquad (4)$$

where M_{cc} is the stress ratio q/p' [$q = (\sigma'_1 - \sigma'_3)$ and $p' = (\sigma'_1 + 2\sigma'_3)/3$ in which σ'_1 and σ'_3 are the major and minor principal effective stresses, respectively] at the critical state in triaxial compression. In the current model formulation, M_{cc} is a model parameter, k_b and k_d are fitting parameters and g(θ) is a function of the Lode's angle θ that determines the shape of the critical-state, bounding and dilatancy surfaces on the deviatoric plane (Loukidis and Salgado 2009).

3 DEVELOPMENT OF THE HIGH STRAIN-RATE CONSTITUTIVE MODEL

Figure 2 illustrates a typical vertical stress-axial strain response of dry Ottawa sand in SHPB test at maximum strain rates of 1000/sec and 2000/sec (data from Veyera and Ross 1995). Three important features of sand stress-strain behavior under impact loading are observed in this

figure which the constitutive model should capture: (1) an inertial response early in the event when the soil sample at rest is suddenly accelerated after initial contact with the striker bar; inertial response becomes more prominent at higher impact velocities (i.e., at higher strain rates), (2) gradual transition from stiff initial inertial response to a viscous flow behavior and (3) a strain hardening behavior at large strains where the stress-strain response looks like an exponentially increasing plot. In this model, feature (1) of the stress-strain curve is captured by shear modulus G while features (2) and (3) are captured by incorporating Perzyna'a flow rule.

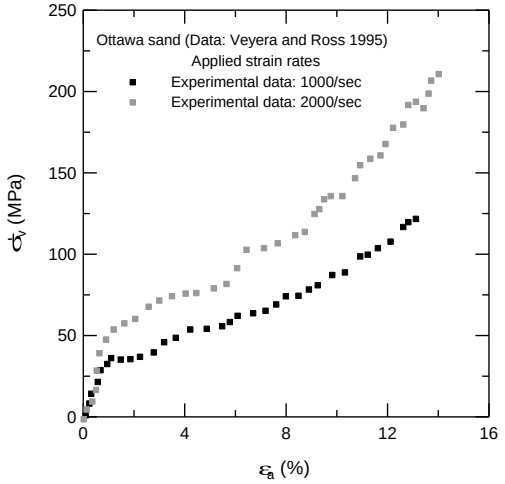

Figure 2. A typical vertical stress-axial strain plot for Ottawa sand in SHPB test (from Veyera and Ross 1995)

3.1 Shear Modulus G

In this model, the stress-strain response is assumed nonlinear elastic inside the yield surface. The SHPB tests on sand (Veyera and Ross 1995, Semblat et al. 1999) show that the shear modulus G is 300-6000 MPa for up to 1% of axial strain, which is almost 5-40% greater than the shear modulus of sand under static loading. This increase in G is due to the inertial response of sand under suddenly applied impact load (as observed by Dupaix and Boyce 2007 for polymers). The experimental data by Matesic and Vucetic (2003) on sand behavior for 0.000002-0.00006/sec strain rate show that G increases by almost 2% over this increase in the strain rate. However, a systematic quantification of the increase of G with strain rate is not yet available for sands at very high strain-rates (1-10^4/sec).

In the current model, we define the shear modulus G at high loading rate by curve fitting through the experimental data. The equation of G under high rate loading is given by

$$G = C_g\left[\ 2.17 - e^{\ 2}\big/\ 1+e\ \right]\sqrt{p'p'_a}\ \ 1+b_{rate}\ln\ 1+\dot{\varepsilon}_{eq} \times \exp\ 1+e_{ij,total}^{iner,lim} - e_{ij,total}\ \ + G_c \qquad (5)$$

where C_g is a model parameter, e is the void ratio, p'$_a$ is a reference mean stress (= 100 kPa), G_c is the constant component of G, $e_{ij,total}$ is the current total deviatoric strain in percent, $e_{ij,total}^{iner,lim}$ is the limit of deviatoric strain in percent when inertia effect becomes maximum and b_{rate} is a parameter that determines the dependence of G on the applied deviatoric strain rate $\dot{\varepsilon}_{eq}$ which is used as a general measure of strain rate as

$$\dot{\varepsilon}_{eq} = \sqrt{\dot{\varepsilon}_{ij}\dot{\varepsilon}_{ij}} \qquad (6)$$

Figure 3 shows the evolution of normalized shear modulus with axial strain at 1000 and 2000/sec strain-rates for Ottawa sand as observed in SHPB tests by Veyera and Ross (1995). The bulk modulus K is related to the small-strain shear modulus G through a constant Poisson's ratio *v* as

$$K = G\frac{2(1+\nu)}{3(1-2\nu)} \qquad (7)$$

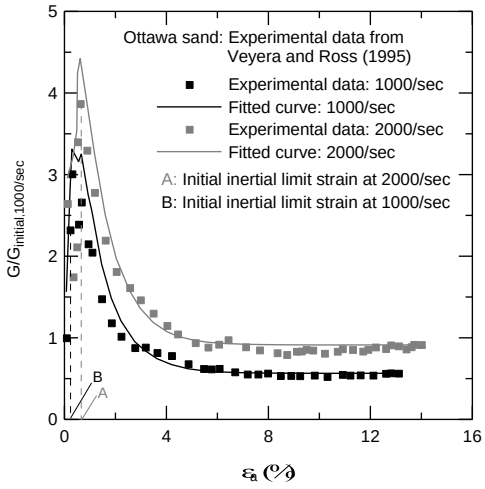

Figure 3. Variation of shear modulus G with axial strain in a SHPB test on Ottawa sand

3.2 Incorporation of Viscoplastic Rate-dependence

The viscoplastic process begins as the stress-state reaches the yield surface. In this paper, Perzyna's overstress theory (Figure 4a) is used to incorporate the viscoplastic behavior of sand. The overstress theory is based on the viscoplastic overstress function ϕ defined as

$$\left\langle \phi\ \ F\ \right\rangle = \begin{cases} F \text{ if } F > 0 \\ 0 \text{ if } F \le 0 \end{cases} \qquad (8)$$

where the parameter F quantifies the amount of overstress and is given by $F = f_d - f_s$ in which f_d and f_s are the dynamic and static yield surfaces, respectively.

Unlike the conventional, single yield-surface plasticity models, there is no static yield surface f_s in our model. In order to use the overstress theory, it is assumed that, at any given instance of time n, the yield surface f, given by equation (1), represents the static yield surface f_s and the "current" stress state, represented by r_n in Figure 4b, is on

f_s. For the next strain increment at time n+1, if the stress state lies outside this static yield surface, then the stress state is viscoplastic. According to Liingaard et al. (2004), the "overstress" is the amount of stress by which a stress state exceeds the yield surface. Therefore, the stress state r_{n+1}^{visco} in Figure 4b, representing the stress state at time n+1, is on a dynamic yield surface f_d and the difference $\left|r_{n+1}^{visco} - r_n\right|$ represents the overstress. The dynamic yield surface is assumed to have the same form as equation (1). Thus, f_d is given by

$$f_d = \sqrt{\rho_{ij}^d \rho_{ij}^d} - \sqrt{2/3}m = 0 \quad (9)$$

where ρ_{ij}^d is the viscoplastic stress ratio, given by

$$\rho_{ij}^d = r_{ij}^d - \alpha_{ij} \quad (10)$$

in which r_{ij}^d is the measure of the current normalized deviatoric stress. Note that ρ_{ij}^d is the amount of "extra" stress from the centre α_{ij} of the yield surface (ρ_{ij}^d represents the distance of r_{n+1}^{visco} from the center of the yield surface in Figure 4b). Therefore, the measure of the overstress $\left|r_{n+1}^{visco} - r_n\right|$ can be obtained by appropriately subtracting the radius m of the yield surface from ρ_{ij}^d. The right hand side of equation (9) for f_d represents this "distance" $\left|r_{n+1}^{visco} - r_n\right|$, and hence, f_d is the overstress in our model. Thus, we choose F = f_d in our model.

Following Perzyna (1966), the total strain rate $\dot{\varepsilon}_{ij}$ is split into elastic and viscoplastic components $\dot{\varepsilon}_{ij}^e$ and $\dot{\varepsilon}_{ij}^{vp}$ as

$$\dot{\varepsilon}_{ij} = \dot{\varepsilon}_{ij}^e + \dot{\varepsilon}_{ij}^{vp} \quad (11)$$

The viscoplastic strain-rate $(\dot{\varepsilon}_{ij}^{vp})$ is given by a non-associated flow rule

$$\dot{\varepsilon}_{ij}^{vp} = \dot{\lambda}_{vp} \, \partial G_{vP} / \partial \sigma_{ij} \quad (12)$$

where G_{vP} is the viscoplastic potential function and $\dot{\lambda}_{vp}$ is the viscoplastic multiplier given by

$$\dot{\lambda}_{vp} = \langle \phi \; F \rangle / \eta \quad (13)$$

in which the parameter η is the viscoplastic coefficient. During the stress-strain integration, the viscoplastic multiplier is determined incrementally as explained in Martindale et al. (2010). The gradient $\partial G_{vP} / \partial \sigma_{ij}$ of the viscoplastic potential in stress space is divided into a deviatoric component R'_{ij} and a mean component that relates to the dilatancy D as (Loukidis and Salgado 2009)

$$\partial G_{vP} / \partial \sigma_{ij} = R'_{ij} + D\delta_{ij}/3 \quad (14)$$

(a)

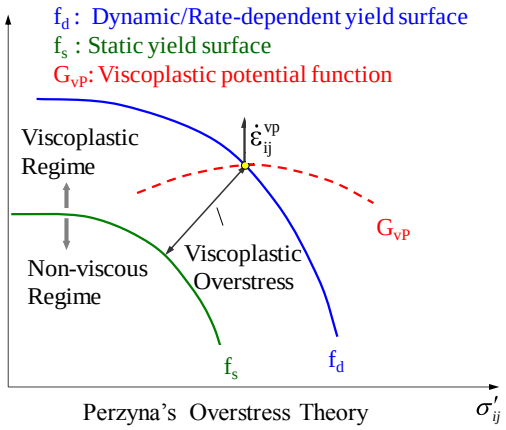

(b)

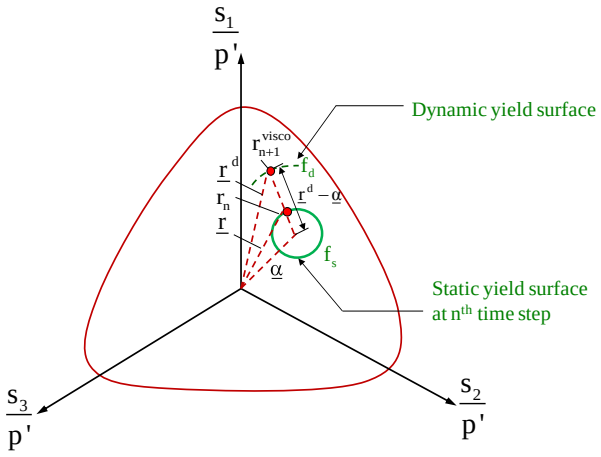

Figure 4. (a) The concept of overstress viscoplastic model (from Liingaard et al. 2004) and (b) initial ('static') and dynamic yield surfaces in the current model

R'_{ij} gives the direction of the deviatoric viscoplastic strain rate $\dot{e}_{ij}^{vp}$. D controls the shear-induced viscoplastic volumetric strain rate $\dot{\varepsilon}_{kk}^{vp}$. The dilatancy D depends on the distance between the current stress state and the projected stress state on the dilatancy surface (Manzari and Dafalias 1997) and is given by

$$D = D_0 / M_{cc} \left(\sqrt{2/3} \; M_d - m \right) - \alpha_{ij} n_{ij} \quad (15)$$

where D_0 is an input parameter controlling the inclination of the stress ratio-dilatancy curve.

The viscoplastic strains due to cap hardening $\dot{\varepsilon}_{ij,cap}^{vp}$ also have volumetric and deviatoric components expressed as

$$\dot{\varepsilon}_{ij,cap}^{vp} = \dot{\lambda}_{vp,cap} \left(1/D^* \right) R'_{ij} + 1/3 \delta_{ij} D^* \quad (16)$$

In equation (16), the volumetric viscoplastic strain component $\varepsilon_{kk,cap}^{vp}$ is equal to the plastic multiplier $\dot{\lambda}_{vp,cap}$ given by

$$\dot{\lambda}_{vp,cap} = 1/H_c \langle \dot{p}' \rangle \quad (17)$$

where H_c is the cap induced plastic modulus and is a function of p_c' – p' and void ratio (p_c' is the crushing pressure). The deviatoric, cap-induced viscoplastic strain rate component $\dot{e}^{vp}_{ij,cap}$ is equal to $\dot{\lambda}_{vp,cap} R'_{ij} / D^*$. The variable D* controls the magnitude of the deviatoric plastic strains relative to the plastic volumetric strains. Hence, D* plays the role of cap-related dilatancy.

3.3 Incorporation of Particle Crushing

Particle crushing of sand under compaction loading is captured in the present model through the incorporation of a flat volumetric hardening cap on the bounding surface. Flat caps have been used by many researchers, both in both classical plasticity (e.g., double hardening models of Vermeer 1978) and bounding surface plasticity models (e.g., Wang et al. 1990, Li 2002). The bounding flat cap is part of the bounding surface, intersecting the hydrostatic axis perpendicularly at $p' = p'_c$ (Figure 5) and is represented mathematically by

$$F_c = p' - p'_c = 0 \quad (18)$$

The variable p'_c has the physical meaning of the crushing pressure for sand which is similar to the preconsolidation pressure in clay. The persistence condition is not applied to the cap because of which stress states marginally outside the cap are possible.

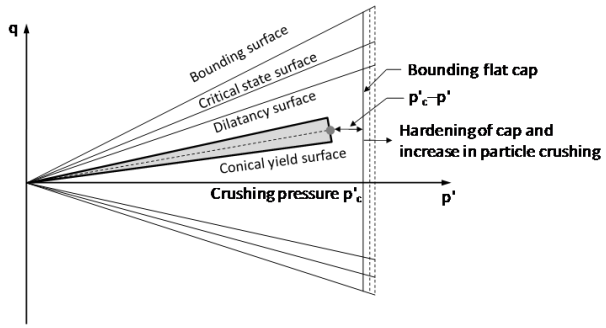

Figure 5. Sand constitutive model in q-p' space

4 MODEL PARAMETERS

The performance of the constitutive model is demonstrated by comparing the stress-strain responses obtained from our model with those obtained from SHPB tests performed by Felice (1985) on New Mexico clayey sand, Semblat et al. (1999) on Fontainebleau sand, and Veyera and Ross (1995) on Ottawa sand. The details of these sands are presented in Table 1.

The rate-independent parameters for Ottawa sand are available from Loukidis and Salgado (2009). We determined the rate-independent model parameters for Fontainebleau sand. For New Mexico clayey sand, the rate-independent model parameters of Ottawa sand were used. The current viscoplastic model formulation has two rate-dependent parameters η and b_{rate}. These parameters are determined by curve-fitting through the SHPB test data (Table 2).

5 MODEL VALIDATIONS

5.1 Split Hopkinson Pressure Bar Test

The developed constitutive model was incorporated in the finite element (FE) software Abaqus through a user material subroutine UMAT. SHPB tests were simulated at different strain rates for the New Mexico clayey sand, Fontainebleau sand and Ottawa sand using Abaqus. Table 1 presents the initial conditions of the SHPB simulations — sample dimension, density, initial void ratio and amplitude of loading, displacement and velocity — as used by Felice (1985) for New Mexico clayey sand, by Veyera and Ross (1995) for Ottawa sand and by Semblat et al. (1999) for Fontainebleau sand. The sand samples were assumed to be completely dry for the simulations. The tests were simulated using an axisymmetic 8-noded full integration element. Zero vertical-displacement and zero radial-displacement conditions were applied at the bottom and side boundaries of the element, respectively. Pressure loading (for New Mexico clayey sand) or displacement boundary condition (for Ottawa sand) or velocity boundary condition (for Fontainebleau sand) was applied on the top boundary of the specimen with exactly similar amplitudes as used in the actual experiments to simulate the uniaxial loading condition of the actual tests. Figure 6 illustrates the geometry and loading of the sample for the New Mexico clayey sand.

The analysis was performed in two steps: (1) geostatic equilibrium and (2) dynamic loading. Although there was no initial confining pressure applied in the actual tests, we applied a minimal initial confining stress of 20 kPa in the geostatic equilibrium stage to avoid numerical singularity. The dynamic loading step is simulated using the implicit dynamic procedure in Abaqus. Damping is applied in the dynamic loading step through material viscoplasticity. Figure 7 shows the vertical stress-strain response of New Mexico clayey sand at 1051/sec strain rate. Figures 8a and 8b show the axial stress-strain response obtained from simulations of Fontainebleau sand and Ottawa sand, respectively, at different strain rates. The peak strengths of sand at high strain rate are predicted reasonably well. The model captures the initial high stiffness of the stress-strain curves for Ottawa sand and Fontainebleau sand. Further investigation is in progress to capture the gradual transition from the initial inertial response to the final exponential response of the curve.

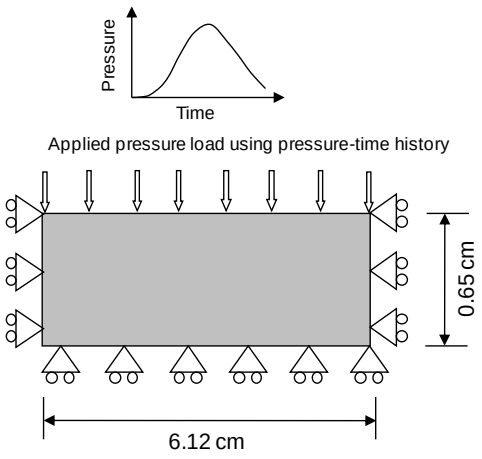

Figure 6. Geometry of the SHPB test sample

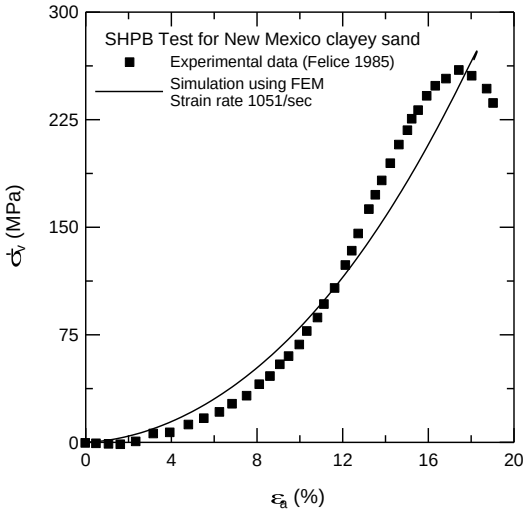

Figure 7. Vertical stress-axial strain stress response of New Mexico clayey sand in SHPB test

Table 1: Description of initial test conditions and loading

Sand	Sample Dimension		Initial void ratio	Applied strain rates	Loading	Source
	Height (cm)	Diameter (cm)				
Ottawa sand	0.635	5.08	0.545	1000/sec, 2000/sec	Applied pressure pulse, peak stress rise time 50 μsec, 257μsec pulse width	Veyera and Ross (1995)
New Mexico clayey sand	0.65	6.12	0.46	1051/sec	Applied pressure pulse, peak stress rise time 100 μsec, 140μsec pulse width	Felice (1985)
Fontainebleau sand	1.00	4.00	0.54 (same as e_{min})	393/sec, 771/sec, 1245/sec	Applied impact velocity, 3.4m/sec, 5.8m/sec, 9.9m/sec	Semblat et al. (1999), Vincens et al. (2003)

Table 2: Description of sands used in model parameter determination and rate-dependent model parameters

Sand	Type	Density (kg/m^3)	CS friction angle (^{o})	Rate-dependent model parameters		Source
				η	b_{rate}	
Ottawa sand	Silica sand	1715	29	0.005	0.002	Veyera and Ross (1995), Yu (2006), Valdes and Koprulu (2007), Graham et al. (2004)
New Mexico clayey sand	Quartz sand	1870	≈ 33	0.005	0.002	Felice (1985), Lancelot (2006), Yu (2006)
Fontainebleau sand	Quartz sand	1667	29	0.005	-0.0001	Semblat et al. (1999), Gaudin et al. (2005), Yu (2006)

(a)

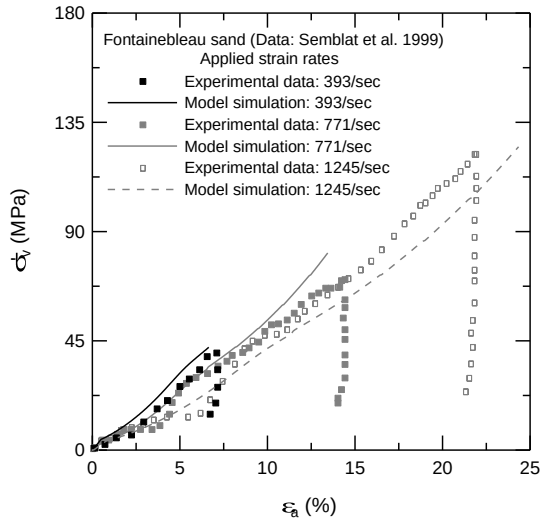

(b)

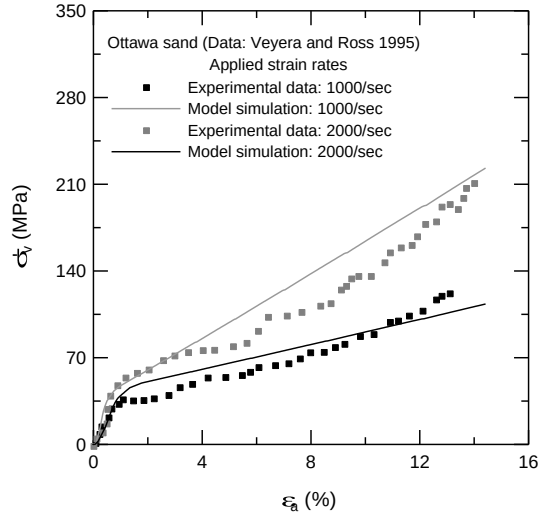

Figure 8. Axial stress-strain response of (a) Fontainebleau sand and (b) Ottawa sand in SHPB test.

6 CONCLUSIONS

The paper presents a viscoplastic constitutive model for sand for geotechnical design against natural and man-made hazards. The model is based on the concepts of critical-state soil mechanics and is developed from an existing rate-independent sand constitutive model with open, "cone"-shaped yield and bounding surfaces. Perzyna's overstress function, the strain-rate dependence of the shear modulus and a flat cap on the bounding surface were added to the existing rate-independent model in order to capture the viscoplastic, rate-dependent behavior of sand and particle breakage. The model is currently capable of simulating sand behavior up to a strain rate of 3000/sec. The peak strength of sand at high loading rates is captured reasonably well. Further investigation is in progress to capture the gradual transition from the initial inertial response to the final exponential response of the stress-strain curve.

The incorporation of the rate-dependence was achieved by using two additional parameters that can be directly determined either through inspection of the experimental data or by fitting simple equations to laboratory test data. The model performance under high loading rate was demonstrated for Ottawa sand, New Mexico clayey sand and Fontainebleau sands. The research outlined in this paper is part of an ongoing research on a systematic study of the mechanical response of soil subjected to extremely high strain rates.

REFERENCES

Barsoum, R. G. S. and Philip, D. 2007. Armor including a strain rate hardening elastomer, *US Patent 7300893*.

Been, K. and Jefferies, M. G. 1985. A state parameter for sands. *Géotechnique*, 35 (2): 99-112.

Casagrande, A., and Shannon, W. L. 1948. Strength of soils under dynamic loads. *Proceedings of the American Society of Civil Engineers*, 74(4): 591–608.

Dafalias, Y. F. and Manzari, M. T. 2004. Simple plasticity sand model accounting for fabric change effects. *Journal of Engineering Mechanics*, *ASCE*, 130: 622- 634.

DeSilva, C. W. 2005. Vibration and shock handbook. *Taylor and Francis, CRC Press*, 1872p.

Dupaix, R. B., and Boyce, M. C. 2007. Constitutive modeling of the finite strain behavior of amorphous polymers in and above the glass transition. *Mechanics of Materials*, 39:39–52.

Felice, C. W. 1985. The response of soil to impulse loads using the split-Hopkinson pressure bar technique. *PhD thesis*, The University of Utah, Utah, USA.

Gaudin, C., Schnaid, F. and Garnier, J. 2005. Sand characterization by combined centrifuge and laboratory tests. *International Journal of Physical Modelling in Geotechnics*, 1: 42-56.

Graham, J., Alfaro, M. and Ferris, G. 2004. Compression and strength of dense sand at high pressures and elevated temperatures. Canadian Geotechnical Journal, 41: 1206–1212.

Grujicic, M., Pandurangan, B, Cheeseman, B. A. 2006. A computational analysis of detonation of buried mines. *Multidiscipline Modeling in Materials and Structures,* 2: 363–387.

Ishihara K. 1996. Soil behaviour in earthquake geotechnics. *Oxford Clarendon Press*, 259-260.

Jackson, J. G., Rohani, B., and Ehrgott, J. Q. 1980. Loading rate effects on compressibility of sand. *Journal of Geotechnical Engineering Division, ASCE*, 106(8): 839–852.

Kumar, S., Chander, R. and Khattri, K.N. 1987. Compressional wave speed in the second crustal layer in Garhwal Himalaya. *Journal of Association of Exploration Geophysicists*, 8(4): 219-25.

Laine, P. and Sandvik. A. 2001. Derivation of mechanical properties for sand., *Proceedings of the 4th Asia–Pacific conference on Shock and Impact Loads on Structures.* Singapore 361–368.

Liingaard, M. Augustesen, A. and Lade, P. V. 2004. Characterization of models for time-dependent behavior

of soils. *International Journal of Geomechanics*, 4(3): 157-177.

Loukidis, D. and Salgado, R. 2009. Modeling sand response using two-surface plasticity. *Computers and Geotechnics*, 36: 166–186.

Manzari, M. T. and Dafalias, Y. F. 1997. A critical state two-surface plasticity model for sands. *Géotechnique*, 47(2): 255-272.

Matešić, L. and Vucetic, M. 2003. Strain-rate effect on soil secant modulus at small cyclic strains. *Journal of Geotechnical and Geoenvironmental Engineering*, *ASCE*, 129 (6): 536–549.

Martindale, H., Higgins, W., Chakraborty, T., Basu, D. 2010. Two-surface viscoplastic sand model for high rate loading. *International Conference on Geotechnical Engineering, ICGE Tunisia.*

Perzyna, P. 1963. The constitutive equations for rate sensitive plastic materials. *Quarterly of Applied Mathematics,* 20: 321-332.

Perzyna, P. 1966. Fundamental problems in viscoplasticity. *Advances in Applied Mechanics*, 9: 244–377.

Semblat, J. F., Phong, L. M. and Gary, G. 1999. 3D-Hopkinson bar: new experiments for dynamic testing on soils. *Soils and foundation*, 39(1): 1-10.

Song, B., Chen, W. and Luk, V. 2009. Impact compressive response of dry sand, *Mechanics of Materials*, 41: 777–785.

Tong, X. and Tuan, C. 2007. Viscoplastic cap model for soils under high strain rate loading. *Journal of Geotechnical and Geoenvironmental Engineering*, *ASCE*, 133(2): 206-214.

Tseng, T. and Chen, W. 2004. Contrasts in seismic wave speeds and density across the 660-km discontinuity beneath the Philippine and the Japan Seas. *Journal of Geophysical Research*, 109: B4, 12 pp.

Vermeer, P. A. (1978) “A double hardening model for sand”, Geotechnique, Vol. 28, No. 4, pp. 413-433.

Veyera, G. E. and Ross, C.A. 1995. High strain rate testing of unsaturated sands using a split-Hopkinson pressure bar, *Proceedings of 3rd International Conference on Recent Advances in Geotechnical Earthquake Engineering and Soil Dynamics*, St-Louis, USA, 31-34.

Vincens, E. Dubujet, Ph. and Cambou, B. 2003. Cyclic behavior of soils, a prediction of permanent deformations. *Deformation Characteristics of Geomaterials*, eds. Di Bendetto et al., Swets & Zeitlinger, Lisse: 1027-1034.

Wang, Z. L., Dafalias, Y. F. and Shen, C. K. (1990). “Bounding Surface Hypoplasticity for Sand.” *Journal of Engineering Mechanics*, *ASCE*, Vol. 116, No. 5, pp. 983-1001.

Wang, Z., Hao, H. and Lu, Y. 2004. A three-phase soil model for simulating stress wave propagation due to blast loading, *International Journal for Numerical and Analytical Methods in Geomechanics*, 28: 33–56.

Whitman, R. V. and Healy, K. A. 1962. Shear strength of sands during rapid loading, *Journal of the Soil Mechanics and Foundations Division*, *ASCE,* 88 SM2: 99-132.

Yamamuro, J. A. and Abrantes, A. E. 2003. Behavior of medium sand under very high strain rates. *Proceedings of 1st Japan-U. S. Workshop on Testing, Modeling, and Simulation*, Boston, MA, USA, 61-70.

Yamamuro, J. A. and Lade, P. V. 1998. Steady-state concepts and static liquefaction of silty sands. *Journal of Geotechnical and Geoenvironmental Engineering*, *ASCE*, 124(9): 868–877.

Yu, H. S. 2006. Plasticity and geotechnics, 524pp, *Springer Publishers*.